

# On-chip quantum interference with heralded photons from two independent micro-ring resonator sources in silicon photonics

Imad I. Faruque, Gary F. Sinclair, Damien Bonneau, John G. Rarity, Mark G. Thompson

Quantum Engineering Technology Labs, H. H. Wills Physics Laboratory & Department of Electrical and Electronic Engineering, University of Bristol, Merchant Venturers Building, Woodland Road, Bristol BS8 1UB, United Kingdom.

E-mail: [imad.faruque@bristol.ac.uk](mailto:imad.faruque@bristol.ac.uk)

17 May 2022

**Abstract.** A heralded single photon source is commonly benchmarked by brightness, purity of the heralded photons and indistinguishability of photons from separate sources. In this paper, we investigated the indistinguishability of micro-ring resonator heralded sources fabricated in the silicon on insulator platform. We demonstrated on-chip quantum interference of heralded single photons at telecom wavelengths, generated from two separate micro-ring resonators, and without any tight spectral filtering. The visibility of the quantum interference was estimated as  $71.89 \pm 3.11\%$  with 95% confidence interval. In addition, we estimated the heralded single-photon purities from each source to be  $86.20 \pm 3.89\%$  and  $78.69 \pm 2.44\%$  by examining the second order correlation of the photon statistics from each source.

## 1. Introduction

The integrated photonics approach to quantum computing requires ideal sources, phase-shifters and detectors integrated alongside fast control electronics [1–4]. An ideal single photon source: emits single photons on demand (deterministic); provides a sufficient rate of single photons (high brightness); emits each heralded photon in a single optical mode (high purity) and has photons from multiple sources indistinguishable from one another (high indistinguishability). In reality, several platforms such as single emitter systems (quantum dots, colour centers etc.) and heralded photon sources based on non-linear optical systems have demonstrated performances approaching that of an ideal source [5]. Despite significant progress, the scalable and controllable integration of multiple indistinguishable single emitters on the same chip with high extraction efficiency and tunability has not yet been demonstrated [6, 7].

In contrast, nonlinear optics based heralded single photon sources can be scalably fabricated but have shortcomings such as being intrinsically non-deterministic and

exhibiting trade-offs among brightness, purity and indistinguishability. Two commonly used nonlinear optical processes, Spontaneous Parametric Down Conversion (SPDC) and Spontaneous Four Wave Mixing (SFWM), require a strong light-matter interaction that depends on the pump-laser brightness and the nonlinear coefficient of the material. By absorbing power from the strong pump field, both SPDC and SFWM generate pairs of photons spontaneously from the vacuum, commonly called signal and idler photons, while conserving energy and momentum of the process. Thus, detecting one photon (signal) from a photon-pair heralds the presence of the other single photon (idler) and acts as an inherently non-deterministic heralded single photon source.

SPDC and SFWM sources can be made very bright by increasing the brightness of the pump laser, however, that will also increase the probability of multi-pair emission which can reduce the indistinguishability for non-photon-number-resolving detectors. The purity of the SPDC and SFWM sources depends on the degree of correlation between signal and idler photons which arises from the energy and momentum conservations. In general, heralding one photon from a photon-pair casts the heralded photon into a mixed state with non-unity purity. Purity can be improved by spectral filtering of the signal and idler photons. In effect, this reduces correlation between signal and idler photons and increases the purity of the heralded photons allowing the observation of over 90% indistinguishability between heralded photons from two separate SPDC [8] or SFWM sources [9]. It follows that, while increasing the purity, narrow spectral filtering reduces the brightness and heralding efficiency [10, 11]. Extensive theoretical and experimental work has been done to mitigate this effect on SPDC and SFWM and to engineer the photon-pair generation with high brightness and heralding efficiency in a pure state without spectral filtering. [12–21]. Most of these systems have not been shown as integrable platforms for scalable and complex circuits except lithium-niobate platforms [22, 23].

Another popular integrated optics platform is silicon photonics due to its mature fabrication technology, reconfigurability and existing roadmaps for CMOS compatible electronic integration [24]. The high nonlinearity of silicon makes the photon pair sources brighter and promises tighter light confinement resulting in small device footprints. In addition to waveguide sources, silicon photonics has well defined resonant structures such as micro-rings and micro-disks which increase the brightness and the purity without the need for tight spectral filtering [25–28]. Comprehensive works on pair generation and purity have been done for these structures. In contrast, interfering independent photons from separate sources—a crucial step towards implementing complex circuits with multiple sources—has been limited to straight waveguides [29–31]. In this work, we interfered heralded photons from two separate micro-ring resonators on chip without any tight spectral filtering, and estimated the visibility  $71.84 \pm 3.11\%$  with 95% confidence interval. We also estimated the purity of each resonator source—with a second order correlation  $g_{xx}^{(2)}(0)$  measurement—leading to an expected  $82.36 \pm 2.25\%$  indistinguishability.

The first part of the paper explores a suitable model for imperfect heralded SFWM

sources and the measurement of indistinguishability (section 2). The second part contains experimental methods and the relevant factors that can affect the quantum interference (section 3). Thereafter, we assess the outcome of this experiment (section 4) and lastly conclude with future directions.

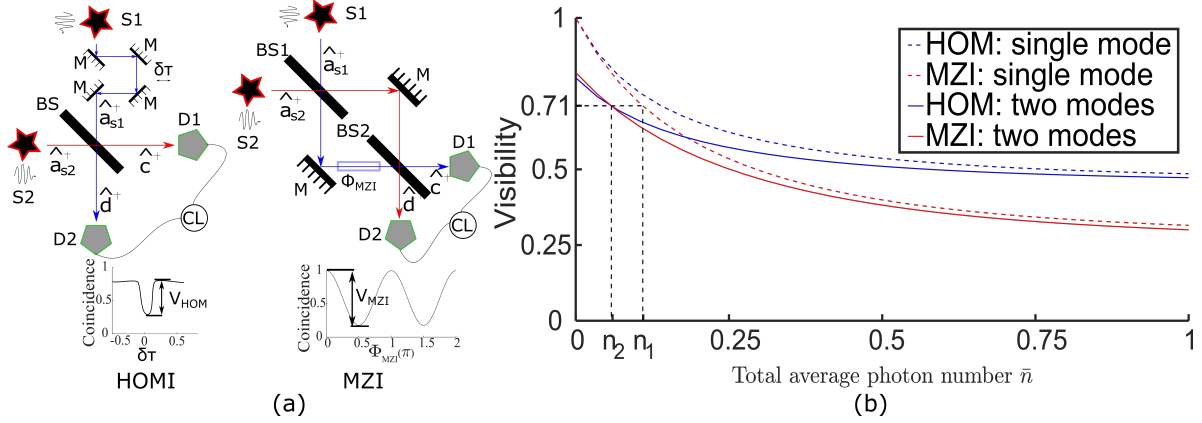


**Figure 1.** Quantum interference of photons from two separate single photon sources S1 and S2. (a) Diagram of Hong-Ou-Mandel Interferometer (HOMI) and Mach-Zehnder Interferometer (MZI) with single photons from S1 and S2. Here,  $\hat{a}_{s1}^\dagger, \hat{a}_{s2}^\dagger, \hat{c}^\dagger, \hat{d}^\dagger$  represents creation operators for corresponding optical modes in  $a, c$  and  $d$ . BS = Beam Splitter, M = mirror. (b) Reduction of visibility (equation 10) of HOMI or MZI due to multi-pair emission (total 10 pairs from both sources) is plotted in terms of average photon numbers generated per pulse. The legend “single mode” refers to pure heralded photons (one optical mode) from each source, and the legend “two modes” refers to impure heralded photons with two effective optical (Schmidt) modes. The graph for HOMI visibility for a single mode (blue dashed line) agrees with the graph reported in reference [29]. The “two modes” graphs are for a purity of  $\sim 82\%$  that corresponds to our experiment with observed visibility of  $\sim 71\%$ . The  $V_{\text{MZI}} = 0.71$  corresponds to average photon numbers  $n_1 = 0.11$  and  $n_2 = 0.06$  for single mode and two modes respectively.

## 2. Effect of multi-pair emission and non-unity purity on indistinguishability of heralded SFWM sources

The degree of indistinguishability is determined by the outcome of quantum interference with heralded photons from separate sources. Quantum interference is defined as a phenomenon where two single photons are incident on a perfectly balanced beam splitter and, based on the interaction of the photons wavepackets, they can exit the beam splitter from the same output port or different output ports. A complete bunching of the photons to one of the output ports of the beam splitter suggests complete indistinguishability of the sources. Consequently, partially indistinguishable sources corresponds to partial photon bunching. Such measure of indistinguishability can be done by any interferometer but in this section we will only discuss calculations involving Hong-Ou-Mandel Interferometer (HOMI) and Mach-Zehnder Interferometer (MZI). The

discussion is based on references [9, 32–34] and is divided into subsections: the relation between SFWM and multimode twin-beam squeezer, the density matrix of heralded single photon source and the equivalence of indistinguishability for HOMI and MZI.

### 2.1. SFWM and multimode twin-beam squeezer

The photon-pair generation through SFWM process can be expressed by the following Hamiltonian operator,

$$\hat{H} = A \int \int d\omega_s d\omega_i f(\omega_s, \omega_i) \hat{a}_s^\dagger \hat{b}_i^\dagger \quad (1)$$

where,  $A$  is a constant proportional to the pump brightness,  $\omega_s$  and  $\omega_i$  are the frequency of the signal and idler photons respectively,  $\hat{a}_s^\dagger$  and  $\hat{b}_i^\dagger$  are creation operators for signal and idler photons respectively, and  $f(\omega_s, \omega_i)$  is the bi-photon function. The latter contains the energy and momentum information of the SFWM process. Often, it is expressed in terms of pump envelope  $\alpha$ , pump frequency  $\omega_p$ , phase (momentum) mismatch  $\Delta k$  and interaction length  $L$ ,

$$f(\omega_s, \omega_i) = \int d\omega_p \alpha(\omega_p) \alpha^*(\omega_s + \omega_i - 2\omega_p) \text{sinc} \left( \frac{\Delta k(\omega_s, \omega_i, \omega_p)L}{2} \right) \quad (2)$$

When the photon-pairs are pure, meaning that signal and idler photons are uncorrelated in color (frequency),  $f(\omega_s, \omega_i)$  is separable in  $\omega_s$  and  $\omega_i$ :  $f(\omega_s, \omega_i) = g(\omega_s) \times h(\omega_i)$ , then the hamiltonian can be rewritten as (Appendix A.1),

$$\hat{H} = r \hat{C}_s^\dagger \hat{C}_i^\dagger + h.c. \quad (3)$$

This is a hamiltonian for single mode twin-beam squeezer [34] with squeezing strength  $r$ , and creation operator for signal and idler photons  $\hat{C}_s^\dagger$  and  $\hat{C}_i^\dagger$  respectively. Therefore, with  $x = \tanh^2(|r|)$  and  $\theta_r = \angle r$ , the wavefunction is expressed in terms of number state basis as,

$$|\Psi\rangle = \exp \left( \frac{-i}{\hbar} \hat{H} \right) |0, 0\rangle \quad (4)$$

$$= \sqrt{1-x} \sum_{n=0}^{\infty} (-e^{j\theta_r})^n \sqrt{x^n} |n, n\rangle \quad (5)$$

In general, the heralded signal photons will be in a state corresponding to non-unity purity and the biphoton function can be expressed in terms of Schmidt decomposition,  $f(\omega_s, \omega_i) = \sum_{k=1}^{\infty} r_k \hat{C}_{sk}^\dagger \hat{C}_{ik}^\dagger$ . Thus the wavefunction can be expressed as a multi-mode squeezer which can be rewritten as a tensor product of the  $k$  single mode twin-beam squeezer with strength  $r_k$  [32, 33],

$$|\Psi\rangle = \otimes_k \exp \left( \frac{-i}{\hbar} \hat{H}_{r_k} \right) |0, 0\rangle \quad (6)$$

$$= \otimes_k \sqrt{1-x_k} \sum_{n_k=0}^{\infty} (-e^{j\theta_{r_k}})^{n_k} \sqrt{x_k^{n_k}} |n_k, n_k\rangle$$

## 2.2. Heralded SFWM sources

Using the wavevector expressions from equation 5 and 6, the density matrix from each source can be expressed as  $\hat{\rho} = |\Psi\rangle\langle\Psi|$ . If the lumped detection efficiency of an idler photon is  $\eta_i$ , and the probability of detecting  $k$  idler photons is  $P_i(k)$  for a generic non-photon-number-resolving detector [35], then the reduced density matrix of the heralded signal photons for single optical mode (unity purity) with normalization constant  $N$  can be written as,

$$\hat{\rho}_s = N \sum_{n=1}^{\infty} P_i(n) \langle n | \hat{\rho} | n \rangle \quad (7)$$

For multi-mode twin-beam squeezer, the reduced density matrix for the signal photons can be expressed by detecting at least one idler photon in at least one of the Schmidt modes  $k$ ,

$$\hat{\rho}_s = N \sum_{\substack{n_1, \dots, n_k=0 \\ n_1 + \dots + n_k \geq 1}}^{\infty} P_i(n_1 + \dots + n_k) \langle n_1 | \dots \langle n_k | \hat{\rho} | n_k \rangle \dots | n_1 \rangle \quad (8)$$

Therefore, the combined density matrix for two sources can be expressed as  $\hat{\rho} = \hat{\rho}_{s1} \otimes \hat{\rho}_{s2}$ .

## 2.3. Equivalence of MZI with HOM interference on indistinguishability

As in figure 1, traditionally, to investigate indistinguishability, the heralded signal photon wavepackets are delayed in time with respect to one another and quantum interference is performed on a beam splitter described as HOMI. As such a long and variable optical delay line is neither possible nor practical due to high loss on chip, a MZI is used to interfere the heralded signal photons from  $\hat{\rho}_{s1}$  and  $\hat{\rho}_{s2}$  as a function of MZI-phase ( $\Phi_{MZI}$ ).

In principal, each source can propagate through an unitary matrix  $U$  corresponding to a photonic circuit describing a general interferometer. While the unitary transfer matrix of a HOMI is a beam splitter with splitting ratio  $\eta_{DC}$ , the MZI can be expressed as a function of splitting ratio of  $\eta_{DC}$  and the phase  $\Phi_{MZI}$ . Therefore, the probability of detecting two heralding idler photons, and heralded signal photons at both of the output modes of the unitary can be recorded as a four-fold coincidence event  $P_{4F}$  describing heralded two-photon quantum interference. Thus, after the unitary transformation,  $\hat{\rho} \xrightarrow{U} \hat{\rho}'$ , the probability of detecting a four-fold event for single optical mode will be,

$$P_{4F} = N_1 N_2 \sum_{\substack{n_{c_1}, \dots, n_{c_k}=0 \\ n_{c_1} + \dots + n_{c_k} \geq 1}}^{\infty} \sum_{\substack{n_{d_1}, \dots, n_{d_k}=0 \\ n_{d_1} + \dots + n_{d_k} \geq 1}}^{\infty} P_s(n_{c_1} + \dots + n_{c_k}) P_s(n_{d_1} + \dots + n_{d_k}) \langle n_{c_1} | \dots \langle n_{c_k} | \langle n_{d_1} | \dots \langle n_{d_k} | \hat{\rho}' | n_{c_1} \rangle \dots | n_{c_k} \rangle | n_{d_1} \rangle \dots | n_{d_k} \rangle \quad (9)$$

where  $P_s(k)$  is the probability of detecting  $k$  signal photons considering a lump detection efficiency  $\eta_s$ , and  $c_k$  and  $d_k$  are output optical modes of the  $U$ . The equation remains similar for multi-modes but with more modes in the outputs. In HOMI, the maximum indistinguishability is found by scanning  $\delta\tau$  and searching the minima of  $P_{4F}$ . This

corresponds to maximum temporal overlap of the signal photons. Similarly, minimum overlap corresponds to distinguishability ( $P_{4F,D}$ ). These values of four-fold coincidence can be used to estimate the visibility and benchmark indistinguishability. In an MZI, the phase  $\Phi_{MZI}$  is scanned to get the minimum and maximum four-fold coincidences which is used to estimate visibility and infer indistinguishability. The visibility of HOMI and MZI are defined as,

$$V_{HOM} = \frac{P_{4F,D} - P_{4F}}{P_{4F,D}} \quad (10a)$$

$$V_{MZI} = \frac{(P_{4F})_{max} - (P_{4F})_{min}}{(P_{4F})_{max} + (P_{4F})_{min}} \quad (10b)$$

For ideal single photon sources, ranging from distinguishable to indistinguishable cases,  $V_{HOM}$  ranges from 0% to 100% while  $V_{MZI}$  ranges from 33% to 100%. Therefore, there is an one to one mapping between the two visibilities of quantum interference which convey the same information about indistinguishability [36, 37].

The visibilities  $V_{HOM}$  and  $V_{MZI}$  from above equations are plotted for imperfect sources in figure 1 with respect to average photon number. The average photon number ( $\bar{n}$ ) is related to squeezing ( $x$ ) through the equation  $\bar{n} = x/(1-x)$  [34]. The plots shows that at higher squeezing (pump power) or average photon number, the contribution from multi-pair emission, such as  $N = 10$  pairs from each source becomes significant and can reduce the visibility appreciably.

In general, exploiting the linearity of the density matrix, an expression for partially indistinguishable sources can be written as a weighted sum of indistinguishable ( $\hat{\rho}_I$ ) and distinguishable ( $\hat{\rho}_D$ ) portion of the  $\hat{\rho}$ ,  $\hat{\rho} = \eta_{ov}\hat{\rho}_I + (1 - \eta_{ov})\hat{\rho}_D$ . Here, the weighting factor  $\eta_{ov}$  defines the overlap between the quantum states of each source. If quantum states of source 1 and source 2 are defined as  $\hat{\rho}_{s1}$  and  $\hat{\rho}_{s2}$  respectively, then the indistinguishable component between them will be the scalar product of these two states,  $\eta_{ov} = tr(\hat{\rho}_{s1}\hat{\rho}_{s2})$ . Thus, the orthogonal component ( $1 - \eta_{ov}$ ) is the distinguishable portion. Subsequently, the interference between heralded signal photons from partially indistinguishable sources can be expressed as,

$$P_{4F} = \eta_{ov}P_{4F,I} + (1 - \eta_{ov})P_{4F,D} \quad (11)$$

This is also an equivalent expression of equation (1) in [38] describing the interference between partially indistinguishable photons. These expressions are effectively valid for one photon-pair emission from each source (Appendix A.3).

### 3. Experimental method

In our experimental setup, as illustrated in figure 2, we interfere on-chip heralded single photons generated in two racetrack micro-ring resonators ( $\Phi_{S1}$  and  $\Phi_{S2}$ ). The leftmost side of figure 2 depicts appropriate pulsed laser light coupled to the chip, in the middle of the figure sits the chip that generates and separates signal-idler photons to herald and interfere the signal photons on chip, and finally the rightmost side of the figure

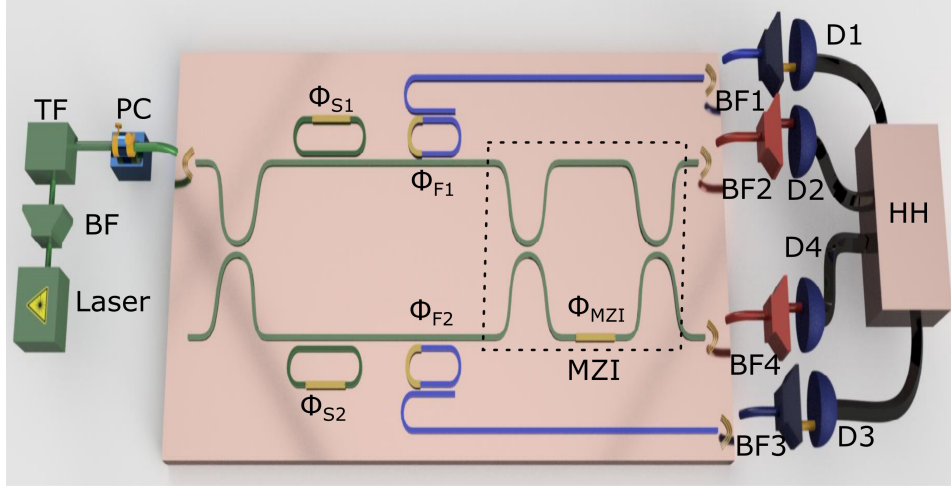


**Figure 2.** The experimental setup contains a laser light which passes through a broadband filter (BF), a tunable bandwidth filter (TF) and a polarisation controller (PC) and coupled to the photonics circuit. The photonic circuit consists of a directional coupler (DC), micro-ring resonator sources ( $\Phi_{S1}$ ,  $\Phi_{S2}$ ), micro-ring filters ( $\Phi_{F1}$ ,  $\Phi_{F2}$ ), MZI composed of DC with reflectivity  $\eta_{MZI}$  (ideally  $\eta_{MZI} = 50\%$ ). Photon-pairs generated by the sources are coupled off-chip and filtered (BF1 to BF4) and collected by single photon detectors (D1 to D4) connected to coincidence logic unit (HH).

consists of off-chip detection mechanism to record the four-fold events corresponding to quantum interference.

In the leftmost side in figure 2 (a), a 50 MHz input pump laser has a pulse width broader than the spectral resonance width of the sources  $\Phi_{S1}$  and  $\Phi_{S2}$  and spectrally tuned on Ch 39 (1546.12 nm) of International Telegraph Union (ITU) frequency grid. The broadband filter (BF) limits the pump photon-leakage into the spectra of generated photon pairs and the tunable bandwidth filter (TF) sufficiently narrows the pump spectrum to be broad enough only at the source resonances. Therefore, BF and TF reduce the background pair production in the coupling waveguides. At this stage an average of 1 mW input power of the laser is coupled into the photonic circuit (coupling loss 4.5 dB) with a suitable polarisation chosen with the polarisation controller (PC).

The very left of the photonic circuit contains a directional coupler (DC) that splits the input light to pump the sources  $\Phi_{S1}$  and  $\Phi_{S2}$ . Both sources are aligned with the pump spectrum such that resonantly enhanced SFWM produces signal-idler photon pairs in Ch31 (1552.52 nm) and Ch47 (1539.77 nm) of the ITU grid. The micro-resonator add-drop filters  $\Phi_{F1}$  and  $\Phi_{F2}$  are only resonant with the idler photons (Ch47), therefore, separates the idler photons through the drop port (violet color waveguides). Subsequently, the idler photons are coupled off chip with coupling loss  $4.5 \text{ dB} \times 2$ , cleaned by filter BF1 and BF3 to reject the pump, detected by single photon detectors D1 and D3 and herald the signal photons (Ch31).

After the MZI interference the signal photons are coupled off-chip (coupling loss  $4.5 \text{ dB} \times 2$ ), filtered (BF2, BF4) to reject the pump and coupled to the single photon

detectors D2 and D4. All four detectors (D1 to D4: average efficiency 75%, dark counts  $< 200$  counts/s) are connected to a PicoQuant timetagger (HydraHarp). The HydraHarp records the photons arrival times which are post processed to identify four-fold coincidence events as heralded two-photon quantum interference as a function of MZI-phase ( $\Phi_{MZI}$ ).

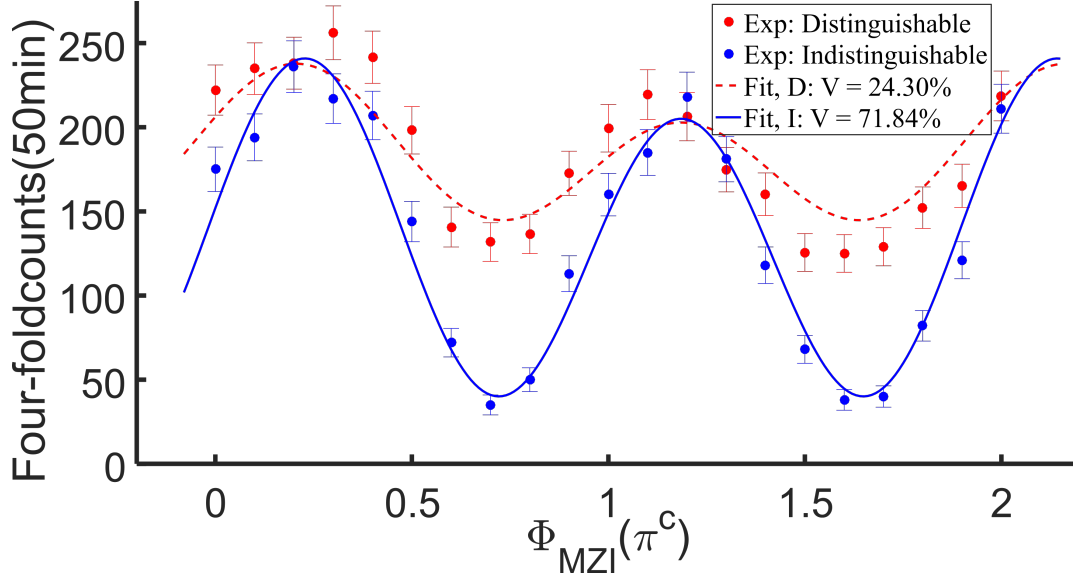


**Figure 3.** Raw four-fold coincidence as a function of  $\Phi_{MZI}$  is the outcome of the experiment. The red events are temporally distinguishable while the blue events are temporally indistinguishable. Fitting the data with equation 11 estimates visibility of 24.30% for distinguishable events and  $71.84 \pm 3.11\%$  for indistinguishable events. The maxima in these fringes have different heights due to the imperfect MZI (Appendix A.2) with the definition of visibility remaining the same.

#### 4. Results and discussion

The MZI fringe that benchmarks the indistinguishability of our heralded sources is shown in figure 3 in terms of the four-fold coincidence events of heralded signal photons as a function of  $\Phi_{MZI}$ . The red events are pairs from separate sources from different pump pulses in time, therefore, temporally distinguishable. It would have led to a MZI visibility of 33% without any multi-pair emission. The blue events are pairs produced by the same pump pulses in time, and for completely indistinguishable and ideal heralded single photon source, would have MZI visibility of 100%. In reality, our sources are not ideal and the visibility is expected to be lower than 100%. Fitting the blue events using the expression of  $P_{4F}$  from equation 11 represented by the blue solid line, the visibility is estimated as  $71.84 \pm 3.11\%$  with  $\eta_{DC} = 39.19 \pm 2.97\%$  with 95% confidence interval. There could be several reasons that the signal photons from  $\Phi_{S1}$  is less than 100% indistinguishable with signal photons from  $\Phi_{S2}$ , such as: non-unity purity, multi-pair contribution, dissimilar temporal dynamics of the sources and technical difficulty

in keeping the sources aligned.

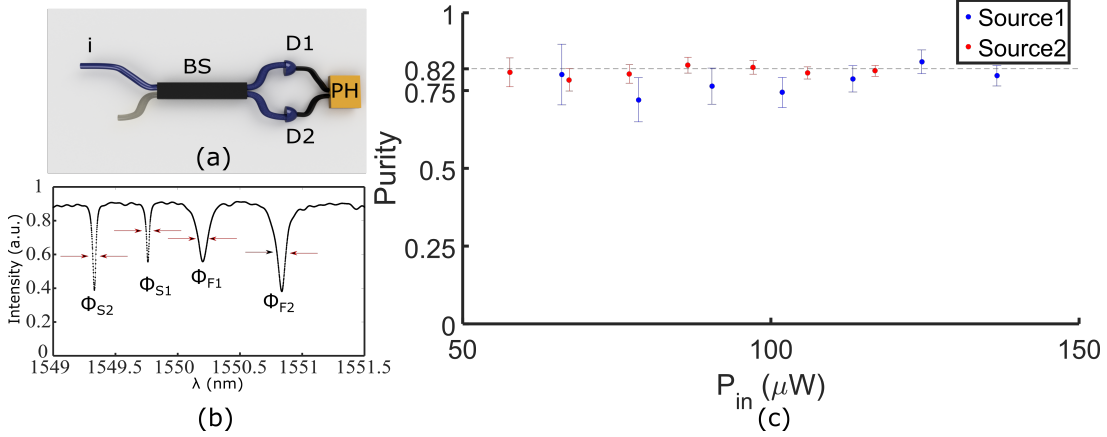


**Figure 4.** (a) Self  $g_{ii}^{(2)}(0)$  of idler photon (“i”) is measured by passing it through a fiber beam splitter (BS with 50% reflectivity) and using detectors D1 and D2 connected to a time interval analyzer (PH) for recording second order correlation. (b) Spectral information of sources  $\Phi_{S1}$ ,  $\Phi_{S2}$  and filters  $\Phi_{F1}$ ,  $\Phi_{F2}$  with corresponding FWHM 30 pm, 26 pm, 92 pm and 82 pm respectively. (c) Purity of one of the sources vs input power shows that purity remains almost the same for a range of power. We did not measure purity at lower power than  $58\mu W$  due to impractical integration time.

The purity of the sources has been estimated by measuring second order correlation function  $g_{ii}^{(2)}(0)$  of the idler photons from each source and using the relation purity,  $P = g_{ii}^{(2)}(0) - 1$  [32] as shown in figure 4. As in the figure, the unheralded idler photons are incident on a 50% reflective beam splitter and the outputs are detected and recorded by a time interval analyzer which estimates the second order correlations. The purity is also measured for different values of pump power and plotted in figure 4. It suggests that the purity values are not affected by the non-linear interactions of the pump power in our range of interest. For our operating power, the estimated purity for both sources are  $P_{S1} = 86.20 \pm 3.89\%$  and  $P_{S2} = 78.69 \pm 2.44\%$ . This, in turn, provides an estimate of the maximum indistinguishability between these sources as  $82.36 \pm 2.25\%$  by using Cauchy-Schwarz inequality,  $tr(\hat{\rho}_{s1}\hat{\rho}_{s2}) \leq \sqrt{tr(\hat{\rho}_{s1}^2)tr(\hat{\rho}_{s2}^2)}$ . Recently, it has been theoretically shown that the purity of a regular resonator, like ours, with equal FWHM for all pump, signal and idler resonances cannot exceed the purity value 93% [39]. Therefore, even in the case of completely identical sources  $\Phi_{S1}$  and  $\Phi_{S2}$ , our purity values indicate the visibility (indistinguishability) of the quantum interference to be lower than estimated 82.36%. In reality,  $\Phi_{S1}$  and  $\Phi_{S2}$  are not identical as shown in figure 4 and the visibility can further degrade. In order to calculate the visibility numerically, we considered Gaussian  $f(\omega_s, \omega_i)$ , and approximated each source with two effective Schmidt modes (Appendix A.5) with the relative strength of the squeezers that corresponds to  $\sim 82\%$  purity.

Considering multi-pair contribution from the sources, the numerically estimated visibility is plotted with respect to average photon number  $\bar{n}$  in figure 1 for pure (single optical mode) and impure ( $\sim 82\%$  purity) with two effective Schmidt modes. The graphs

indicates that  $\sim 71\%$  visibility of MZI corresponds to average photon number  $\bar{n} = 0.11$  and  $0.06$  for single mode and two mode states respectively for each source. Analyzing two-fold coincidence counts as a function of optical input power, our source 1 and source 2 have estimated  $\bar{n}_1 = 0.093 \pm 0.001$  and  $\bar{n}_2 = 0.123 \pm 0.001$  with  $68\%$  confidence interval (Appendix A.4). Figure 1 indicates that the average of these two values  $\bar{n} = 0.183$  for each source indicates  $\sim 60\%$  and  $\sim 55\%$  visibility for single and two modes respectively. Appendix A.3 outlines a simpler method to estimate the indistinguishability in terms of  $\eta_{ov}$  between two sources from the measured visibility using an analysis involving only one photon-pair from each source.

Thus, combination of the two aforementioned effects: multi-pair emission and impurity can reduce the visibility to our measured value of  $\sim 71\%$ . While the impurity alone estimates the visibility as  $82.36\%$ , the additional effect of multi-pair emission reduces it to  $\sim 71\%$  from  $82.36\%$  which is a significant reduction of  $86\%$ . However, the preceding analysis and figure 1 suggest that our methods are either overestimating the average photon number  $\bar{n}$  from each source, or underestimating the purity of both sources. Further experiments are required to resolve it.

In addition to multi-pair emission and purity, the temporal dynamics of the ring-resonators can cause visibility degradation. The temporal dynamics of the non-identical sources can cause them to go in and out of spectral overlap [40]. The imperfect directional coupler ( $\eta_{DC}$ ) at the beginning of the photonic circuit causes different pumping of the two sources making the nonlinear interaction inside the cavities different from each other. All of these will make the heralded signal photons of one source different from the other at a particular time instance.

Technically, the most challenging part of this experiment is to keep the sources  $\Phi_{S1}$  and  $\Phi_{S2}$  spectrally overlapped while the  $\Phi_{MZI}$  heater is swept from  $0 \text{ mW}$  ( $\Phi_{MZI} = 0^\circ$ ) to  $60 \text{ mW}$  ( $\Phi_{MZI} = 2\pi^\circ$ ). This is due to a combination of two effects. The first one is the high quality factor (small FWHM shown in Fig 4) of the resonators which makes them very sensitive to environmental changes. Second one is the thermal crosstalk among the components of the photonic circuit. The latter effect means when the  $\Phi_{MZI}$  heater dissipates reasonable amount of heat, the heat propagates to  $\Phi_{S1}$ ,  $\Phi_{S2}$  and shift their resonances. Therefore, along with the temperature controller, a thorough characterization of heat compensation was required to keep  $\Phi_{S1}$  and  $\Phi_{S2}$  overlapped at any configuration for the whole duration of the experiment.

## 5. Conclusion

Our current results on quantum interference between individual silicon micro-ring resonators are a step towards building more complicated quantum photonic devices. We found that the parameters of the pump lasers together with the design parameters (FWHM, coupling etc) of the resonators affect the indistinguishability significantly. For example, the peak power of the pump determines the contribution from the multi-pair emission while the spectral shape of the pulse affects the purity while the quality factor

of the resonators plays an important role for controlling their spectral position as well as scalable fabrication. Further experiments on the preceding examples are required to determine the optimum criteria.

The model used for this experiment explains, within experimental margin of error, the effect of the non-unity purity and the multi-pair emission on the measurement of indistinguishability. This model can be further improved by: implementing loss in the photon pairs which escapes the resonators and estimating the effect of non-identical temporal dynamics.

## Acknowledgments

This work was supported by the Marie Curie Actions within the Seventh Framework Programme for Research of the European Commission, under the Initial Training Network PICQUE, Grant No. 608062, in addition to EPSRC, ERC, BBOI, US Army Research Office (ARO) Grant No. W911NF-14-1-0133. M.G.T. and J.G.R. acknowledge fellowship support from the Engineering and Physical Sciences Research Council (EPSRC, UK).

## Appendix

This appendix will annex the calculations on: the SFWM and multimode twin-beam squeezer in terms of density matrix formalism; the heralded signal photon propagating through the MZI for quantum interference and estimation of mean photon number (squeezing) and equivalent number of the Schmidt modes.

### Appendix A.1. SFWM and twin beam squeezer

According to interaction picture of quantum mechanics, the wavefunction  $|\Psi\rangle$  corresponding to the SFWM process will be,

$$|\Psi\rangle = \exp\left(\frac{-i}{\hbar}\hat{H}\right) |0,0\rangle \quad (\text{A.1})$$

where, the vacuum for signal and idler photon is expressed as  $|0\rangle_s|0\rangle_i = |0,0\rangle$ . Now, when the heralded signal photons are pure, the biphoton function does not contain correlated spectral information between signal and idler photons. Essentially, it means  $f(\omega_s, \omega_i)$  is separable in  $\omega_s$  and  $\omega_i$ ,  $f(\omega_s, \omega_i) = g(\omega_s) \times h(\omega_i)$ . Therefore rearranging the quantities in the hamiltonian  $\hat{H}$ , the wavefunction can be expressed as,

$$|\Psi\rangle = \exp\left(\frac{-i}{\hbar}\left(r\hat{C}_s^\dagger\hat{C}_i^\dagger + h.c.\right)\right) |0,0\rangle \quad (\text{A.2})$$

where,  $r$  is a scalar related to pump brightness,  $h.c.$  refers to hermitian conjugate and,

$$\hat{C}_s^\dagger = \int d\omega_s g(\omega_s) \hat{a}_s^\dagger \quad (\text{A.3})$$

$$\hat{C}_i^\dagger = \int d\omega_i h(\omega_i) \hat{a}_i^\dagger \quad (\text{A.4})$$

This is a general expression of single mode twin-beam squeezer and the wavefunction, with  $x = \tanh^2(|r|)$  and  $\theta_r = \angle r$ , can be expressed in terms of number state basis as,

$$|\Psi\rangle = \sqrt{1-x} \sum_{n=0}^{\infty} (-e^{j\theta_r})^n \sqrt{x^n} |n, n\rangle \quad (\text{A.5})$$

Following section 2.1, the heralded signal photon will be in a mixed state corresponding to non-unity purity. Subsequently, using Schmidt decomposition, the biphoton function  $f(\omega_s, \omega_i)$  can be expressed as a sum of orthogonal basis functions of signal and idler photons,  $f(\omega_s, \omega_i) = \sum_{k=1}^{\infty} r_k \hat{C}_{sk}^\dagger \hat{C}_{ik}^\dagger$ . Thus the wavefunction can be expressed as a tensor product of the single mode twin beam squeezer with strength  $r_k$ ,

$$\begin{aligned} |\Psi\rangle &= \otimes_k \exp\left(\frac{-i}{\hbar} \left(r_k \hat{C}_{sk}^\dagger \hat{C}_{ik}^\dagger - h.c.\right)\right) |0, 0\rangle \\ &= \otimes_k \sqrt{1-x_k} \sum_{n_k=0}^{\infty} (-e^{j\theta_{r_k}})^{n_k} \sqrt{x_k^{n_k}} |n_k, n_k\rangle \end{aligned} \quad (\text{A.6})$$

Therefore, the density matrix  $\hat{\rho} = |\Psi\rangle\langle\Psi| = \otimes_k \hat{\rho}_k$ , where  $\hat{\rho}_k$  is the density matrix of each Schmidt mode  $k$ .

If the lumped detection efficiency of a idler photon is  $\eta_i$ , and the probability of detecting  $n$  idler photon is  $P_i(n)$  for a generic non photon-number-resolving detector [35],

$$P_i(n) = 1 - (1 - \eta_i)^n \quad (\text{A.7})$$

Then for single optical mode, the reduced density matrix for the heralded signal photons with normalization constant  $N$  can be written as,

$$\hat{\rho}_s = N \sum_{n=1}^{\infty} P_i(n) \langle n | \hat{\rho} | n \rangle \quad (\text{A.8})$$

For multi-mode twin-beam squeezer, the reduced density matrix for the signal photons can be expressed by detecting at least one idler photon in at least one of the Schmidt modes  $k$ ,

$$\hat{\rho}_s = N \sum_{\substack{n_1, \dots, n_k=0 \\ n_1 + \dots + n_k \geq 1}}^{\infty} P_i(n_1 + \dots + n_k) \langle n_1 | \dots | n_k | \hat{\rho} | n_k \rangle \dots | n_1 \rangle \quad (\text{A.9})$$

Therefore, the combined density matrix for two sources can be expressed as  $\hat{\rho} = \hat{\rho}_{s1} \otimes \hat{\rho}_{s2}$ . After the unitary transformation of MZI or HOMI, the new density matrix will be  $\hat{\rho}'$ ,  $\hat{\rho} \xrightarrow{U} \hat{\rho}'$ . At this point, through the unitary transformation, the heralded signal photons from both sources experience quantum interference and are distributed into the two output optical modes of the unitary  $U$ . Considering we have detected at least one photon in each idler modes from each sources for heralding, and now, detecting at least one photon in both of these optical modes corresponds to a four-fold coincidence event

$P_{4F}$  as,

$$P_{4F} = N_1 N_2 \sum_{\substack{n_{c_1}, \dots, n_{c_k} = 0 \\ n_{c_1} + \dots, n_{c_k} \geq 1}}^{\infty} \sum_{\substack{n_{d_1}, \dots, n_{d_k} = 0 \\ n_{d_1} + \dots, n_{d_k} \geq 1}}^{\infty} P_s(n_{c_1} + \dots, n_{c_k}) P_s(n_{d_1} + \dots, n_{d_k}) \langle n_{c_1} | \dots \langle n_{c_k} | \langle n_{d_1} | \dots \langle n_{d_k} | \hat{\rho}' | n_{c_1} \rangle \dots | n_{c_k} \rangle | n_{d_1} \rangle \dots | n_{d_k} \rangle \quad (\text{A.10})$$

Where,  $c_k$  and  $d_k$  represent all possible output modes of the  $U$  depending on distinguishable or indistinguishable transformations. For multi-mode case, the expression remains the same but with more optical modes in the output of the unitary. Thus, plotting  $P_{4F}$  with respect to relative time delay  $\delta\tau$  between two signal photons we get a characteristic graph for HOMI. Similarly plotting  $P_{4F}$  with respect to relative phase  $\Phi_{MZI}$  between the two interferometric path we get a typical graph for MZI. The resulting graphs can estimate indistinguishability by modeling in terms of overlap parameter  $\eta_{ov}$ .

Using this model for single optical mode: limiting total  $N = 3$  pairs from both sources, we re-derived the expression of HOMI visibility in reference [9] and limiting total  $N = 10$  pairs from both sources we reproduced the graph of visibility as a function of average photon number mentioned in reference [29].

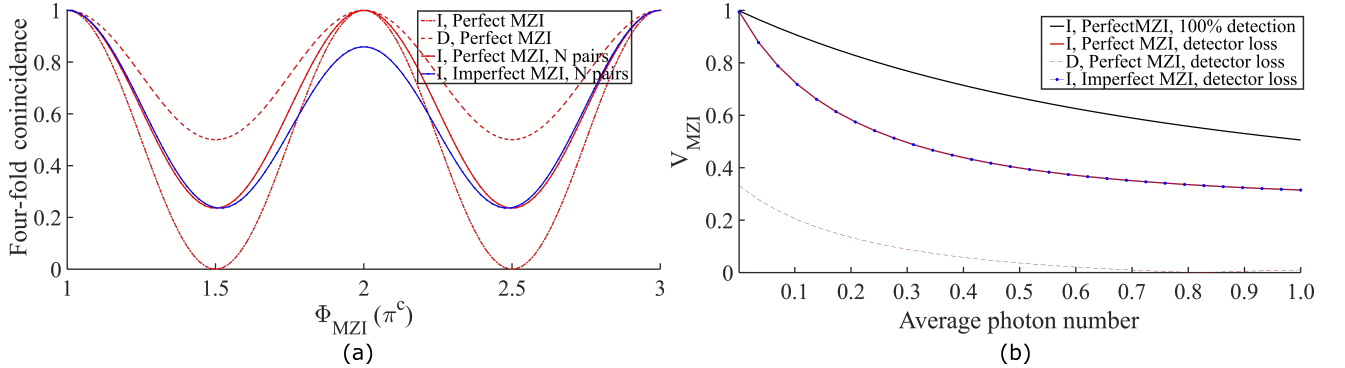


**Figure A1.** MZI fringes and visibility for perfect ( $\eta_{MZI} = 50\%$ ) and imperfect ( $\eta_{DC} = 39\%$ ) MZI and for distinguishable (D) and indistinguishable (I) signal photons: (a) MZI fringes as a function of  $\Phi_{DC}$  for different configuration. (b) Visibility of MZI as a function of average photon number for different configuration.

### Appendix A.2. Indistinguishability estimated by MZI

The unitary transfer matrix of the MZI can be expressed as a function of  $\eta_{DC}$  and  $\Phi_{MZI}$ ,

$$U(\eta_{DC}, \Phi_{MZI}) = \begin{bmatrix} \sqrt{\eta_{DC}} & \sqrt{1 - \eta_{DC}} \\ \sqrt{1 - \eta_{DC}} & -\sqrt{\eta_{DC}} \end{bmatrix} \begin{bmatrix} e^{i\Phi_{MZI}} & 0 \\ 0 & 1 \end{bmatrix} \begin{bmatrix} \sqrt{\eta_{DC}} & \sqrt{1 - \eta_{DC}} \\ \sqrt{1 - \eta_{DC}} & -\sqrt{\eta_{DC}} \end{bmatrix} \quad (\text{A.11})$$

$$= \begin{bmatrix} U_{11} & U_{12} \\ U_{21} & U_{22} \end{bmatrix} \quad (\text{A.12})$$

In Heisenberg picture, the creation operators of the signal photons of each source ( $\hat{a}_{s1}^\dagger$ ,  $\hat{a}_{s2}^\dagger$ ) can be the input modes of the unitary. They will be transformed into

output modes  $\hat{a}_1^\dagger, \hat{a}_2^\dagger, \hat{a}_3^\dagger$  and  $\hat{a}_4^\dagger$  depending on the indistinguishability of the sources. For distinguishable sources, they will transform into different output modes,

$$\hat{a}_{s1}^\dagger \rightarrow U_{11}\hat{c}_1^\dagger + U_{12}\hat{d}_1^\dagger \quad (\text{A.13})$$

$$\hat{a}_{s2}^\dagger \rightarrow U_{21}\hat{c}_2^\dagger + U_{22}\hat{d}_2^\dagger \quad (\text{A.14})$$

For indistinguishable case, the transformation will contain same output modes  $\hat{c}_1^\dagger$  and  $\hat{d}_1^\dagger$ ,

$$\hat{a}_{s1}^\dagger \rightarrow U_{11}\hat{c}_1^\dagger + U_{12}\hat{d}_1^\dagger \quad (\text{A.15})$$

$$\hat{a}_{s2}^\dagger \rightarrow U_{21}\hat{c}_1^\dagger + U_{22}\hat{d}_1^\dagger \quad (\text{A.16})$$

Using these transformation and using equation 9, the four-fold coincidence as a function of  $\Phi_{MZI}$  (MZI fringe) can be analytically evaluated for completely distinguishable ( $P_{4F,D}$ ) sources and partially indistinguishable ( $P_{4F}$ ) sources. The corresponding visibilities as a function of average photon number can be calculated from equation 10b and is plotted in figure A1. Here, the loss  $\eta_s = \eta_i = 0.01$ . For a perfect heralded sources with only one photon pair emission at single photon Fock state, the equations simplifies to more recognizable set of equations,

$$P_{4F,D} = N_1 N_2 (|U_{11}U_{22}|^2 + |U_{12}U_{21}|^2) \quad (\text{A.17})$$

$$P_{4F,I} = N_1 N_2 |U_{11}U_{22} + U_{12}U_{21}|^2 \quad (\text{A.18})$$

These can be used in equation 11 to estimate the overlap,  $\eta_{ov}$  between the two sources,

$$P_{4F} = N_1 N_2 (\eta_{ov} \times |U_{11}U_{22} + U_{12}U_{21}|^2 + (1 - \eta_{ov}) \times (|U_{11}U_{22}|^2 + |U_{12}U_{21}|^2)) \quad (\text{A.19})$$

For perfect and balanced MZI (the splitting ratio  $\eta_{DC} = 50\%$ ), this further reduces to  $P_{4F,D} = |\cos^2(\Phi_{MZI}/2)|^2 + |\sin^2(\Phi_{MZI}/2)|^2$  and  $P_{4F,I} = |\cos(\Phi_{MZI})|^2$ . These are plotted as dotted red lines in figure A1. The visibility for the red-dot line (indistinguishable case) is 100% and for the red-dash line (distinguishable case) is 30%. Introducing multi-pair emission gives the solid red line with reduced visibility. When the splitting ratio  $\eta_{DC} \neq 50\%$ , the interference cannot redistribute the energy completely to destructive and constructive interferences for all values of  $\Phi_{MZI}$  and we get slightly smaller maxima for those values of phase represented by the solid blue line. Such imperfection of MZI leaves the visibility definition unchanged. The visibility for the aforementioned scenarios can be plotted with respect average photon number of the both sources.

### Appendix A.3. Visibility for multimode twin-beam squeezer

Let's consider the simplest multi-mode twin beam squeezer: two-Schmidt mode for each source with maximum one photon-pair in each optical mode. The wavefunction for source 1 with two Schmidt mode of squeezing strength  $x_{11}$  and  $x_{12}$  can be expressed in the Fock basis as,

$$|\Psi_{s1}\rangle = \sqrt{1-x_{11}} \sum_{n=0}^{\infty} (-e^{j\theta_{r11}})^n \sqrt{x_{11}^n} |n, n\rangle \otimes \sqrt{1-x_{12}} \sum_{m=0}^{\infty} (-e^{j\theta_{r12}})^m \sqrt{x_{12}^m} |m, m\rangle \quad (\text{A.20})$$

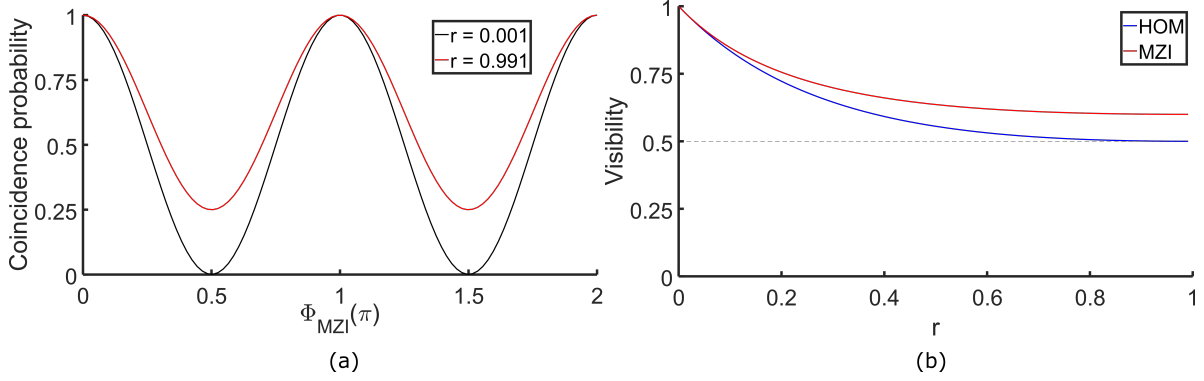


**Figure A2.** Visibility of perfect MZI and HOMI for heralded sources with two Schmidt modes emitting only one photon-pair at a time from each source. Depending on the value of purity,  $r$  varies from 0 to 1. (a) MZI fringes as a function of  $\Phi_{MZI}$  for two values of  $r$ . Smaller value of  $r$  corresponds to almost pure while larger value of  $r$  reflects impure states. (b) Visibility of HOMI and MZI as a function of  $r$  shows visibility reduction for decreasing purity (increasing  $r$ ).

Heralding at most one idler photon in each mode and total one photon from each source, the reduced density matrix for signal photons from source 1 becomes,

$$\hat{\rho}_{s1} = N_1 P_i(1) [x_{11} (|1\rangle\langle 1|_{11} \otimes |0\rangle\langle 0|_{12}) + x_{12} (|0\rangle\langle 0|_{11} \otimes |1\rangle\langle 1|_{12})] \quad (\text{A.21})$$

Here,  $N_1$  is the normalisation constant and  $P_i(1)$  is the detection probability of one idler photon. Similarly, the reduced density matrix for signal photons from source 2 with squeezing strengths  $x_{21}$  and  $x_{22}$  can be expressed as,

$$\hat{\rho}_{s2} = N_2 P_i(1) [x_{21} (|1\rangle\langle 1|_{21} \otimes |0\rangle\langle 0|_{22}) + x_{22} (|0\rangle\langle 0|_{21} \otimes |1\rangle\langle 1|_{22})] \quad (\text{A.22})$$

Therefore, the combined density matrix for the whole system can be written as  $\hat{\rho} = \hat{\rho}_{s1} \otimes \hat{\rho}_{s2}$ . Any term in this density matrix can be rewritten using creation and annihilation operator, such as  $|1\rangle\langle 1|_{11} \otimes |1\rangle\langle 1|_{22} = \hat{a}_{11}^\dagger \hat{a}_{22}^\dagger |0\rangle\langle 0|_{11} \otimes |0\rangle\langle 0|_{22} \hat{a}_{11} \hat{a}_{22}$ . Here,  $\hat{a}_{jk}^\dagger, \hat{c}_{jk}^\dagger, \hat{d}_{jk}^\dagger$  are creation operators and  $\hat{a}_{jk}, \hat{c}_{jk}, \hat{d}_{jk}$  are annihilation operators for  $jk$  optical modes at the input/output of the unitary. The system can evolve according to the unitary transformation  $U$  as  $\hat{\rho} \xrightarrow{U} \hat{\rho}'$  for completely distinguishable case,

$$\begin{aligned} \hat{a}_{11}^\dagger &\rightarrow U_{11}\hat{c}_{11}^\dagger + U_{12}\hat{d}_{11}^\dagger & \hat{a}_{12}^\dagger &\rightarrow U_{11}\hat{c}_{12}^\dagger + U_{12}\hat{d}_{12}^\dagger \\ \hat{a}_{21}^\dagger &\rightarrow U_{21}\hat{c}_{21}^\dagger + U_{22}\hat{d}_{21}^\dagger & \hat{a}_{22}^\dagger &\rightarrow U_{21}\hat{c}_{22}^\dagger + U_{22}\hat{d}_{22}^\dagger \end{aligned}$$

Following the procedure outlined in Appendix A.1, the probability of four-fold coincidence for temporally distinguishable events become,

$$P_{4F.D} = N_1 N_2 P_i(1)^2 P_s(1)^2 (|U_{11}U_{22}|^2 + |U_{12}U_{21}|^2) (x_{11}x_{21} + x_{11}x_{22} + x_{12}x_{21} + x_{12}x_{22}) \quad (\text{A.23})$$

For indistinguishable sources, there are two options:

- (i) Source 1 and source 2 are completely indistinguishable. It means that the primary Schmidt mode 11 and 21 of source 1 and 2 respectively will result into the same

**Table A1.**  $\eta_{ov}$  estimation.

Case	$V$ (%)	$\eta_{ov}$ (%)	$\eta_{DC}$ (%)
Pure heralded source	$71.84 \pm 3.11$	$67.63 \pm 10.99$	$39.19 \pm 2.97$
Impure and one-pair	$71.90 \pm 3.00$	$86.33 \pm 14.09$	$39.19 \pm 2.97$

optical mode, and similarly secondary Schmidt mode 12 and 22 of source 1 and 2 respectively will transform into the same optical modes:

$$\begin{aligned} \hat{a}_{11}^\dagger &\rightarrow U_{11}\hat{c}_{11}^\dagger + U_{12}\hat{d}_{11}^\dagger & \hat{a}_{12}^\dagger &\rightarrow U_{11}\hat{c}_{12}^\dagger + U_{12}\hat{d}_{12}^\dagger \\ \hat{a}_{21}^\dagger &\rightarrow U_{21}\hat{c}_{11}^\dagger + U_{22}\hat{d}_{11}^\dagger & \hat{a}_{22}^\dagger &\rightarrow U_{21}\hat{c}_{12}^\dagger + U_{22}\hat{d}_{12}^\dagger \end{aligned}$$

Therefore, the four-fold coincidence probability will be,

$$\begin{aligned} P_{4F} = N_1 N_2 P_i(1)^2 P_s(1)^2 &\left( |U_{11}U_{22} + U_{12}U_{21}|^2 (x_{11}x_{21} + x_{12}x_{22}) \right. \\ &\left. + (|U_{11}U_{22}|^2 + |U_{12}U_{21}|^2) (x_{11}x_{22} + x_{12}x_{21}) \right) \end{aligned} \quad (\text{A.24})$$

- (ii) Source 1 optical modes can be decomposed into orthogonal Schmidt modes of Source 2. It means that the primary Schmidt mode of source 1, mode 11 can be expressed in terms of primary Schmidt mode of source 2, mode 21 with proper weighting factors  $x_{jk}$ . The sub-Schmidt modes of both sources, modes 12 and 22 are orthogonal to each other and everything else. If the purity of source 1 is  $P_1$  and source 2 is  $P_2$ , then the weighting factors will be:  $x_{11} = \eta_{ov}\sqrt{P_1}$ ,  $x_{12} = 1 - \eta_{ov}\sqrt{P_1}$ ,  $x_{21} = \sqrt{P_2}$  and  $x_{22} = 1 - \sqrt{P_2}$ . Then the density matrices for both sources can be relabeled as,

$$\hat{\rho}_{s1} = N_1 P_i(1) (x_{11}\hat{\rho}_I + x_{12}\hat{\rho}_{Ds1}) \quad (\text{A.25})$$

$$\hat{\rho}_{s2} = N_2 P_i(1) (x_{21}\hat{\rho}_I + x_{22}\hat{\rho}_{Ds2}) \quad (\text{A.26})$$

If we take the inner product of the density matrices of both sources, we get

$$\begin{aligned} \text{tr}(\hat{\rho}_{s1}\hat{\rho}_{s2}) &= x_{11} \times x_{21} \\ &= \eta_{ov}\sqrt{P_1}\sqrt{P_2} \end{aligned} \quad (\text{A.27})$$

The unitary transformation for this scenario will be,

$$\begin{aligned} \hat{a}_{11}^\dagger &\rightarrow U_{11}\hat{c}_{11}^\dagger + U_{12}\hat{d}_{11}^\dagger & \hat{a}_{12}^\dagger &\rightarrow U_{11}\hat{c}_{12}^\dagger + U_{12}\hat{d}_{12}^\dagger \\ \hat{a}_{21}^\dagger &\rightarrow U_{21}\hat{c}_{11}^\dagger + U_{22}\hat{d}_{11}^\dagger & \hat{a}_{22}^\dagger &\rightarrow U_{21}\hat{c}_{22}^\dagger + U_{22}\hat{d}_{22}^\dagger \end{aligned}$$

Therefore, with  $x_{11}x_{21} = \eta_{ov}\sqrt{P_1}\sqrt{P_2}$  and  $x_{11}x_{22} + x_{12}x_{21} + x_{12}x_{22} = 1 - \eta_{ov}\sqrt{P_1}\sqrt{P_2}$ , the four-fold coincidence probability will be,

$$\begin{aligned} P_{4F} = N_1 N_2 P_i(1)^2 P_s(1)^2 &(\eta_{ov}\sqrt{P_1}\sqrt{P_2} \times |U_{11}U_{22} + U_{12}U_{21}|^2 \\ &+ (1 - \eta_{ov}\sqrt{P_1}\sqrt{P_2}) \times (|U_{11}U_{22}|^2 + |U_{12}U_{21}|^2)) \end{aligned} \quad (\text{A.28})$$

The above can be used for equation 11 to estimate the overlap,  $\eta_{ov}$  between the two sources with two Schmidt modes.

As the overlap parameter  $\eta_{ov}$  determines how much of the indistinguishable part of the density matrix  $\hat{\rho}_I$  contributes to the fringe, it gives an estimate of the indistinguishability of the sources except that it's value strongly depends on the implementation of  $\hat{\rho}_s$ . We have implemented two different  $\rho_s$  to evaluate  $\eta_{ov}$ : a pure heralded source with only one photon-pair emitted at a time (equation A.19) and an impure (two Schmidt modes) source with only one photon-pairs at a time from each source (equation A.28). These scenarios estimates the same visibility as they fit the same fringe, but depending on the portion of the fringe that  $\hat{\rho}_I$  alone can assimilate, we obtain different values of  $\eta_{ov}$  in table A1.

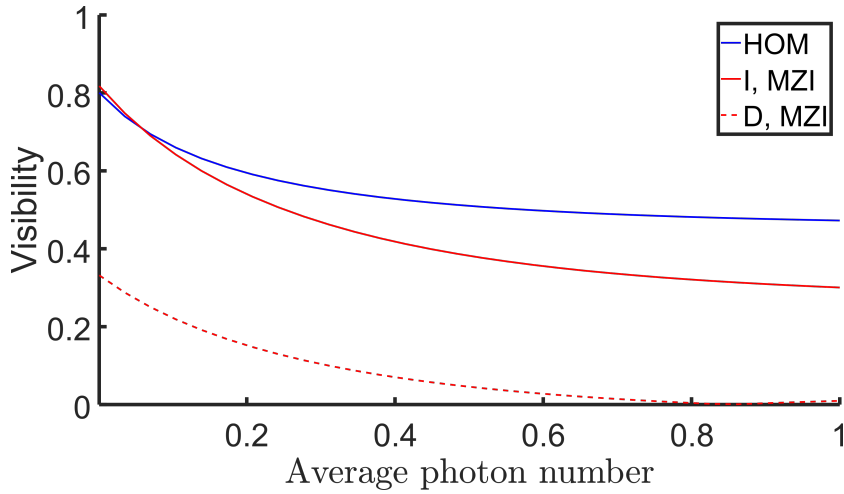


**Figure A3.** Visibility as a function of average photon number  $\bar{n}$  for perfect MZI and HOMI of heralded sources with two Schmidt modes. The total number of photon-pairs emitted from both sources at a time is limited to 10, and the detection loss is set to  $\eta_s = \eta_i = 0.01$  matching our experiment. For two-mode squeezer the values chosen for  $r_1 = r_2 = 1/8$  correspond to  $\sim 82\%$  purity. The general trend of all the curves are very similar: reduction in visibility due to multi-pair contribution.

Assuming same squeezing for both sources,  $x_{11} = x_{21} = y$  and  $x_{12} = x_{22} = r \times y$ , the visibility for HOMI takes a simple form as in equation A.30 and plotted in figure A2. Here,  $r$  is the relative strength between the two squeezer of each source and can be estimated from the purity. It shows that unlike the 100% visibility for pure sources with only one photon-pair, the impure sources has the visibility strongly dependent on the purity (the parameter  $r$ ) for both of the above scenarios:

$$V_{HOM} = \frac{1 + r^2}{(1 + r)^2} \quad (\text{A.29})$$

$$V_{HOM} = \frac{r^2}{(1 + r)^2} \quad (\text{A.30})$$

A simpler expression for prefect MZI can be obtained showing strong dependence of the visibility on purity for the second scenario,

$$P_{4F} = N_1 N_2 P_i(1)^2 P_s(1)^2 y^2 (r^2 |\cos(\phi)|^2 + (1 + 2r)(|\cos^2(\phi)|^2 + |\sin^2(\phi)|^2)) \quad (\text{A.31})$$

**Table A2.** Loss and average photon number estimation.

Source	$\eta_s$	$\eta_i$	$\bar{n} = \frac{\gamma}{R}$
1	0.0146	0.0362	$0.0925 \pm 0.0091$
2	0.0132	0.0243	$0.1233 \pm 0.0097$

Consequently, the density matrices for each sources with multi-pair emission cannot be simply divided into distinguishable and indistinguishable portions as in equation A.28. Extending the above model for multi-pair emission and numerically calculating in-total 10 photon-pairs at a time from both sources, we can see the degradation in visibility due to both multi-pair emission and non-unity purity as plotted in figure A3.

#### Appendix A.4. Estimating average photon number

If the lumped efficiency of the four wave mixing process is  $\gamma$ , probability of photon pair generation per pulse is  $p$  and repetition rate of the laser is  $R$ , then the equations for detecting only signal photons, only idler photons and signal-idler coincidences from each sources can be written as,

$$P(s) = (\eta_s \gamma) p^2 + \beta_s p + DC_s \quad (\text{A.32})$$

$$P(i) = (\eta_i \gamma) p^2 + \beta_i p + DC_i \quad (\text{A.33})$$

$$P(s, i) = (\eta_i \eta_s \gamma) p^2 + ACC \quad (\text{A.34})$$

Here,  $DC$  represents dark counts and  $ACC$  represents accidentals. The factor  $\gamma$  is proportional to the the strength of the non-linearity of the silicon and the peak power of the pump.  $\gamma$  lumps the total SFWM strength of the system. Fitting the above equation with the experimental data,  $\gamma$  can be estimated. Then the average photon pair generated per pulse will be,  $\bar{n} = \gamma/R$ . Our source 1 and source 2 have estimated  $\bar{n}_1 = 0.093 \pm 0.001$  and  $\bar{n}_2 = 0.123 \pm 0.001$  with 68% confidence interval.

#### Appendix A.5. Estimating number of Schmidt modes and squeezing from purity

Considering Gaussian joint-spectral amplitude from biphoton function  $f(\omega_s, \omega_i)$ , the relative distribution of the squeezers of the multimode non-pure heralded state can be expressed as a single parameter equation [32]. The equation relates the relative squeezing of each mode  $\lambda_k$  with a parameter  $\mu$  as  $\lambda_k = \sqrt{1 - \mu^2} \mu^k$ . Here,  $\sum \lambda_k^2 = 1$  and the parameter  $\mu$  can be estimated from the self- $g^{(2)}$ -measurements via  $\mu = \sqrt{2/g^{(2)} - 1}$ . Therefore, using the  $g^{(2)}$  values for source 1 and source 2, we can plot the relative contribution of multimode squeezers for each sources as depicted in figure A4. According to this plot, we can conclude that including upto two Schmidt modes for each of our sources is a reasonable approximation.

If the the total average photon number for source 1 is  $\bar{n}_1$  and average photon number for each Schmidt mode is  $\bar{n}_{11}, \bar{n}_{12}$  with corresponding squeezing of  $x_{11}, x_{12}$ , then knowing

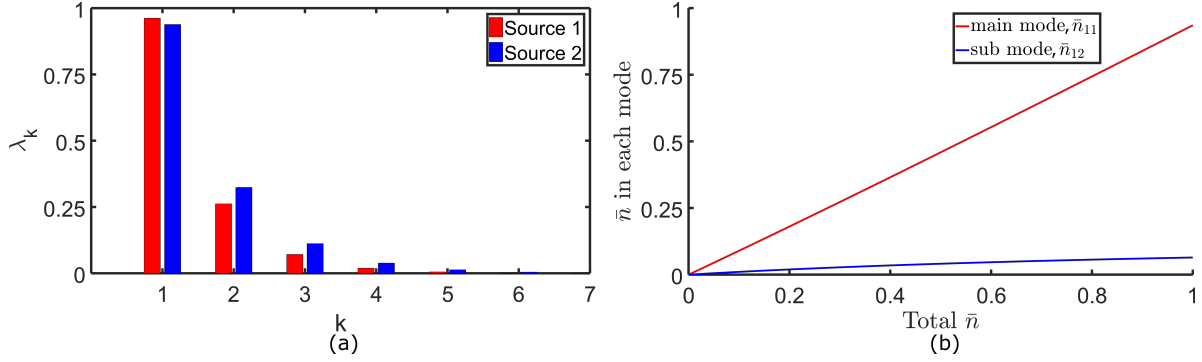


**Figure A4.** The relative strength of squeezers vs the  $k^{\text{th}}$  optical mode for multimode squeezed state for each source in (a). Using these values, we can solve for the average photon number in each Schmidt mode for a particular value of total average photon number  $\bar{n}$  as plotted in (b).

$r_1 = x_{12}/x_{11}$  from purity value (figure A4) and  $\bar{n}_1$  from coincidence measurement, we can solve for  $\bar{n}_{11}$ ,  $\bar{n}_{12}$ :

$$n_1 = n_{11} + n_{12} \quad (\text{A.35})$$

$$n_{11} = \frac{x_{11}}{1 - x_{11}} \quad (\text{A.36})$$

$$n_{12} = \frac{x_{12}}{1 - x_{12}} \quad (\text{A.37})$$

## References

- [1] O’Brien J L 2007 *Science* **318** 1567–1570 ISSN 0036-8075 (*Preprint* 0803.1554) URL <http://www.ncbi.nlm.nih.gov/pubmed/18063781><http://www.sciencemag.org/content/318/5856/1567><http://www.sciencemag.org/cgi/doi/10.1126/science.1142892>
- [2] Varnava M, Browne D E and Rudolph T 2008 *Physical Review Letters* **100** 1–4 ISSN 00319007 (*Preprint* 0702044)
- [3] Kaltenbaek R, Prevedel R, Aspelmeyer M and Zeilinger A 2009 *Physical Review A - Atomic, Molecular, and Optical Physics* **79** 1–4 ISSN 10502947 (*Preprint* 0809.3991)
- [4] Mendoza G J, Santagati R, Munns J, Hemsley E, Piekarek M, Martín-López E, Marshall G D, Bonneau D, Thompson M G and O’Brien J L 2016 *Optica* **3** 127 ISSN 2334-2536 URL <http://dx.doi.org/10.1364/OPTICA.3.000127><https://www.osapublishing.org/abstract.cfm?URI=optica-3-2-127>
- [5] Ding X, He Y, Duan Z C, Gregersen N, Chen M C, Unsleber S, Maier S, Schneider C, Kamp M, Höfling S, Lu C Y and Pan J W 2016 *Arxiv Preprint* ISSN 10797114 (*Preprint* 1601.00284) URL <http://arxiv.org/abs/1601.00284>
- [6] Aharonovich I, Englund D and Toth M 2016 *Nature Photonics* **10** 631–641 ISSN 1749-4885 URL <http://www.nature.com/doi/10.1038/nphoton.2016.186>
- [7] Eisaman M D, Fan J, Migdall A and Polyakov S V 2011 *Review of Scientific Instruments* **82** 071101 ISSN 0034-6748 URL <http://aip.scitation.org/doi/10.1063/1.3610677>
- [8] Aboussouan P, Alibert O, Ostrowsky D B, Baldi P and Tanzilli S 2010 *Physical Review A - Atomic, Molecular, and Optical Physics* **81** ISSN 10502947 (*Preprint* 0912.5312)
- [9] Fulconis J, Alibert O, Wadsworth W J and Rarity J G 2007 *New Journal of Physics* **9** ISSN 13672630 (*Preprint* 0701129)

- [10] Meyer-Scott E, Montaut N, Tiedau J, Sansoni L, Herrmann H, Bartley T J and Silberhorn C 2017 1–11 (*Preprint* 1702.05501) URL <http://arxiv.org/abs/1702.05501>
- [11] Castelletto S, Degiovanni I P, Schettini V and Migdall a 2006 *Metrologia* **43** S56–S60 ISSN 0026-1394 (*Preprint* 0601067v2)
- [12] U'Ren A B, Silberhorn C, Erdmann R, Banaszek K, Grice W P, Walmsley I a and Raymer M G 2006 *Laser Phys.* **15** 2005 14 ISSN 1054660X (*Preprint* 0611019) URL <http://arxiv.org/abs/quant-ph/0611019>
- [13] Mosley P J, Lundeen J S, Smith B J, Wasylczyk P, U'Ren A B, Silberhorn C and Walmsley I a 2008 *Physical Review Letters* **100** 1–4 ISSN 00319007 (*Preprint* 0711.1054)
- [14] Harder G, Ansari V, Brecht B, Dirmeier T, Marquardt C and Silberhorn C 2013 *Optics Express* **21** 13975 ISSN 1094-4087 (*Preprint* arXiv:1304.6635v2) URL <http://www.opticsexpress.org/abstract.cfm?URI=oe-21-12-13975>
- [15] Cassemiro K N, Laiho K and Silberhorn C 2010 *New Journal of Physics* **12** 0–15 ISSN 13672630 (*Preprint* 1007.2599)
- [16] Laudenbach F, Hübel H, Hentschel M, Walther P and Poppe A 2016 *Optics express* **24** 19–26
- [17] Grice W, U'Ren a and Walmsley I 2001 *Physical Review A* **64** 1–7 ISSN 1050-2947
- [18] Bruno N, Martin A, Guerreiro T, Sanguinetti B and Thew R T 2014 *Optics Express* **22** 1481–1484 ISSN 10944087 (*Preprint* 1403.6740) URL <http://www.opticsinfobase.org/oe/abstract.cfm?uri=oe-22-14-17246>
- [19] Jin R b, Gerrits T, Fujiwara M, Wakabayashi R, Yamashita T, Miki S, Terai H, Shimizu R, Takeoka M and Sasaki M 2015 **2** 1–8 (*Preprint* arXiv:1507.02424v1)
- [20] Spring J B, Mennea P L, Metcalf B J, Humphreys P C, Gates J C, Rogers H L, Soller C, Smith B J, Kolthammer W S, Smith P G R and Walmsley I A 2016 *Submitted to Science (unpublished)* (*Preprint* 1603.06984)
- [21] Spring J U B, Ennea P A L M, Etcalf B E J M, Umphreys P E C H, Ates J A C G, Ogers H E L R, Öller C H S, Mith B R J S, Olthammer W S T K, Mith P E G R S and Almsley I A N A W 2017 1–9
- [22] Alibart O, D'Auria V, De Micheli M, Doutre F, Kaiser F, Labonté L, Lunghi T, Picholle É and Tanzilli S 2016 *Journal of Optics* **18** 104001 ISSN 2040-8978 (*Preprint* 1608.01100) URL <http://stacks.iop.org/2040-8986/18/i=10/a=104001?key=crossref.490a5ead8f284783a007073b7fdee740>
- [23] Sharapova P R, Luo K H, Herrmann H, Reichelt M, Meier T and Silberhorn C 2017 1–13 (*Preprint* 1704.03769) URL <http://arxiv.org/abs/1704.03769>
- [24] Silverstone J, Damien B, Jeremy L O and Mark G T *IEEE JOURNAL OF SELECTED TOPICS IN QUANTUM ELECTRONICS* ISSN 07338724 URL <http://ieeexplore.ieee.org/stamp/stamp.jsp?arnumber=7479523>
- [25] Helt L G, Yang Z, Liscidini M and Sipe J E 2010 *Optics letters* **35** 3006–3008 ISSN 0146-9592
- [26] Garay-Palmett K, Jeronimo-Moreno Y and U'Ren A B 2013 *Laser Physics* **23** 015201 ISSN 1054-660X (*Preprint* 1309.2705) URL <http://arxiv.org/abs/1309.2705>
- [27] Grassani D, Simbula A, Pirota S, Galli M, Menotti M, Harris N C, Baehr-Jones T, Hochberg M, Galland C, Liscidini M and Bajoni D 2016 *Scientific reports* **6** 23564 ISSN 2045-2322 (*Preprint* 1602.04962) URL <http://www.nature.com/srep/2016/160401/srep23564/full/srep23564.html>
- [28] Lu X, Jiang W C, Zhang J and Lin Q 2016 *Arxiv Preprint* (*Preprint* arXiv:1602.08057v1)
- [29] Harada K i, Takesue H, Fukuda H, Tsuchizawa T, Watanabe T, Yamada K, Tokura Y and Itabashi S i 2011 *New Journal of Physics* **13** 065005 ISSN 1367-2630 URL <http://stacks.iop.org/1367-2630/13/i=6/a=065005?key=crossref.dac4a4d8dc6512cb0c3fc0e5ed4b6af2>
- [30] Xiong C, Bell B and Eggleton B J 2016 *Nanophotonics* **0** ISSN 2192-8614 URL <http://www.degruyter.com/view/j/nanoph.ahead-of-print/nanoph-2016-0022/nanoph-2016-0022.xml>
- [31] Zhang X, Jiang R, Bell B, Choi D Y, Chae C and Xiong C 2016 *Technologies* **4** 25 ISSN 2227-7080

- URL <http://www.mdpi.com/2227-7080/4/3/25>
- [32] Christ A, Laiho K, Eckstein A, Cassemiro K N and Silberhorn C 2011 *New Journal of Physics* **13** ISSN 13672630 (*Preprint* 1012.0262)
- [33] Maurerer W, Avenhaus M, Helwig W and Silberhorn C 2009 *Physical Review A - Atomic, Molecular, and Optical Physics* **80** 1–5 ISSN 10502947 (*Preprint* 0812.3597)
- [34] Gerry C C and Knight P L 2005 *Introductory Quantum Optics*. ISBN 9780521820356 (*Preprint arXiv:1011.1669v3*)
- [35] Kok P and Braunstein S L 2000 *Physical Review A* **61** 042304 ISSN 1050-2947 (*Preprint* 9903074) URL <http://link.aps.org/doi/10.1103/PhysRevA.61.042304>
- [36] Rarity J G, Tapster P R, Jakeman E, Larchuk T, Campos R a, Teich M C and Saleh B E a 1990 *Physical Review Letters* **65** 1348–1351 ISSN 00319007
- [37] Ou Z Y, Zou X Y, Wang L J and Mandel L 1990 *Physical Review A* **42** 2957–2965 ISSN 10502947
- [38] Loredo J C, Broome M A, Hilaire P, Gazzano O, Sagnes I, Lemaitre A, Almeida M P, Senellart P and White A G 2016 *ArXiv* 1–9 (*Preprint* 1603.00054) URL <http://arxiv.org/abs/1603.00054>
- [39] Vernon Z, Menotti M, Tison C C, Steidle J A, Fanto M L, Thomas P M, Preble S F, Smith A M, Alsing P M, Liscidini M and Sipe J E 2017 *Arxiv Preprint* 1–5 (*Preprint* 1703.10626) URL <http://arxiv.org/abs/1703.10626>
- [40] Pelc J S, Rivoire K, Vo S, Santori C, Fattal D a and Beausoleil R G 2014 *Optics Express* **22** 3797 ISSN 1094-4087 URL <https://www.osapublishing.org/oe/abstract.cfm?uri=oe-22-4-3797>